A DEPTH-AVERAGED $\mu(I)$ MODEL FOR DENSE SNOW AVALANCHES

Callum Tregaskis[1]*, Peter Gauer[1] and Dieter Issler[1]

[1] Norwegian Geotechnical Institute, Oslo, Norway

ABSTRACT: Observations from large-scale avalanche test sites indicate velocity measurements are not always adequately captured by widely used rheological models and friction laws, such as the Voellmy–Salm approach used in RAMMS::Avalanche and other avalanche software, available for consultancy. This has a significant impact in two key areas of hazard mitigation and assessment: (i) the mobility of the avalanche can be under-predicted, thus, leading to a high uncertainty in the hazard zones (ii) the design and assessment of mitigation measures like dams and fences is affected, as the effectiveness and economic impact are directly tied to the pressures the measure has to account for. To make progress on this front, we need to look to the physics controlling the granular behaviour of dry-snow avalanche flows but not compromise on the benefits of depth-averaged methodologies, for instance, the ability to model avalanche areas at a large scale without detrimental computation time and resources needed to complete avalanche simulations. There is now ample evidence from laboratory experiments that the $\mu(I)$-rheology describes dry, dense granular flows very well. Here, μ is the internal friction and I is the inertial number, which can be thought of as a non-dimensionalised shear rate. By utilising such a rheology in a depth-averaged setting, it is possible to maintain computational efficiency at a geophysical scale whilst including a more sophisticated, and realistic, frictional behaviour of the avalanche. In this paper, we compare experimental measurements from the Ryggfonn test site in Norway to simulations with a prototype depth-averaged $\mu(I)$ avalanche model parameterised for snow avalanches. The material properties of the snowpack in the model link to the parameters in the friction law, allowing an avenue for material effects to be included. By including additional considerations for varying topography, and erosion, entrainment and deposition of material, the model presented here is of direct relevance for hazard zoning and modelling of snow avalanches in mountainous areas.

KEYWORDS: Snow avalanche dynamics, numerical modelling, depth-averaged modelling.

1 INTRODUCTION

Measurements at large-scale avalanche test sites show that the Voellmy–Salm friction law, widely used in avalanche flow models for consultancy, systematically underestimates velocity, and thus, key characteristic properties of the avalanche, such as impact pressure and avalanche flow mobility, may be underestimated in hazard assessments. This is especially critical in the design of mitigation measures like dams, where evaluating the mobility of the avalanche and its potential impact pressures is key, but also, in the planning phase of new infrastructure in mountainous areas, where accurately capturing the area of impact from the avalanche is essential.

*Corresponding author address:
Callum Tregaskis, Norwegian Geotechnical Institute, P.O. Box 3930 Ullevål Stadion, 0806 Oslo, Norway;
tel: +4741214950;
e-mail: callum.tregaskis@ngi.no

The Voellmy–Salm model utilises a friction law with two key parameters that dictate the frictional behaviour of the flow, namely the Coulomb friction parameter μ in addition to a turbulent frictional parameter ξ. This frictional description leads to a bed shear stress term of the form

$$\tau_b = -\frac{\bar{\boldsymbol{u}}}{|\bar{\boldsymbol{u}}|}\left(\mu g' h + k\bar{\boldsymbol{u}}^2\right), \tag{1}$$

where the Voellmy parameters (μ and $\xi = g/k$) are typically chosen by statistical analysis of historical avalanches (Voellmy, 1955; Issler et al., preprint). The parameter ζ here denotes the local slope angle, h the local flow depth, and g' the slope normal component of the gravitational acceleration g. The reason for the discrepancy is that the drag term in the Voellmy–Salm model increases with the square of velocity ($\bar{u}$), which severely limits the velocity that an avalanche can attain. This is an important effect, however, to capture the behaviour of flowing granular materials, such as dense snow avalanches, which tend towards a terminal velocity given a sustained incline. While Voellmy-type

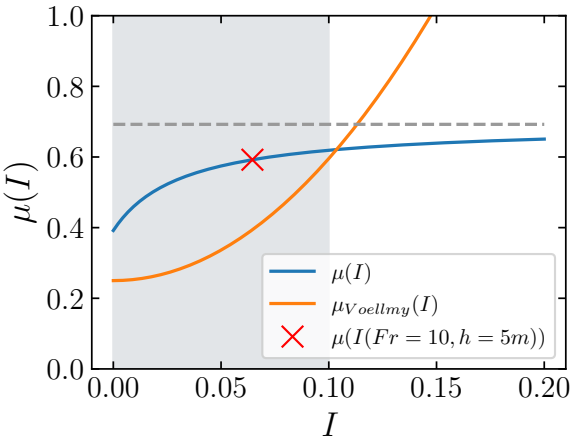


Fig. 1: Shows a $\mu(I)$ curve, using the dense flow parameterisation (see, table 1:2), against the Voellmy–Salm approach, converted to a function of I by assuming a Bagnold profile through the depth and a typical flow height of 3 m. The grey region indicates an approximation for the likely range of I reached by dense snow avalanches.

models do present this behaviour, the results are in stark contrast to experiments with dry granular flows which show a sub-linear increase in drag with velocity (or, more precisely, the shear rate) (GDR-MiDi, 2004). Thus, in some cases, particularly in dry snow avalanche runout simulations, unphysical values of the Voellmy parameters are needed to account for the discrepancy caused by this effect.

The behaviour of the drag in dry granular flow experiments is very well captured by the so-called $\mu(I)$-rheology, where μ is the internal friction coefficient and I the inertial number, which can be thought of as a non-dimensionalised shear rate. Figure 1 demonstrates the discrepancy between the two approaches. Here equation (1) has been adapted to be written in terms of the inertial number I by assuming a depth-averaged Bagnold velocity profile through the depth and a fixed flow height of 3 m, as follows

$$\bar{u} = \frac{2}{5}\frac{I_\zeta}{d}\sqrt{\Phi g \cos\zeta}\, h^{\frac{3}{2}}. \qquad (2)$$

Here we have assumed d = 1 cm for the mean grain diameter and ϕ = 0.6 for the solids volume concentration of the dense avalanche core. I_ζ is the inertial number which is constant through the depth, given a specific slope angle (Gray and Edwards, 2014). The μ and ξ parameters were specified using the values in table 1:1 for a typical avalanche run in Norway.

Recently, this rheological model has been extended beyond the stationary flows of the original experiments (GDR-MiDi, 2004) to include approximations for the quasi-static shearing just before a flow comes to a rest and for the very rapid collisional regime at high speeds (Holyoake and McElwaine, 2012; Barker et al., 2021). This gives scope for this description of the rheology to include more complex phenomenology in avalanches such as levee and other deposit formations (Edwards et al., 2017; Tregaskis et al., 2022) but also to include high-speed effects such as increased mobility, rollwaves and fluidisation (Edwards and Gray, 2015; Breard et al., 2022). By utilising this in a depth-averaged setting, it is possible to maintain computational efficiency even for large-scale avalanches whilst describing a more realistic frictional behaviour of the avalanche.

In this paper, we show a prototype depth-averaged μ(I) flow model, parameterised for snow avalanches and adapted to include complex terrain effects, as well as erosion and deposition effects for snow. Using this approach changes the focus from statistical evaluation of parameters from runout distances to parameterisation through material properties of the snow, which can change drastically from wet, dense avalanches to dry powder-snow avalanches. This change from a historically calibrated model to one capturing more of the physics of the material has an increasing importance with the rapidly changing climate affecting common avalanche conditions and frequencies (see *e.g.*, Eckert et al., 2010).

A new model parameterisation is constructed using data from full-scale avalanche tests, and the model is compared against three sets of experimental measurements from avalanches with differing runout characteristics from the Ryggfonn test site in Norway. Using an idealised parameterisation for snow, the new model captures the characteristics of the three runout scenarios for the dense flow. Its key advantages are the following:

(i) The model parameters relate directly to snow properties one can measure in the field.

(ii) The model can capture the experimentally observed shear-rate dependence and hysteretic effects of dense snow avalanches.

A further benefit of this approach is that it opens a route to capturing more complex effects in the avalanche flow, for instance, the change from a dense to a fluidised flow regime in dry-snow avalanches or where water or other interstitial fluids play a role in the flow dynamics.

2 METHODS

2.1 The mathematical model

The mass and momentum conservation laws can be stated in terms of the terrain-following curvilinear coordinate system, allowing the model to be used on complex terrain as dictated by a digital elevation model (DEM). In this coordinate system, where x, y are orthogonally aligned to the input topography projection lines, the depth-averaged mass and momentum conservation laws for the avalanche thickness $h(x, y, t)$ (measured normal to the surface) and the depth-averaged velocity $\bar{\boldsymbol{u}}(x, y, t) = (\bar{u}(x, y, t), \bar{v}(x, y, t))$ are

$$\frac{\partial h}{\partial t} + \nabla \cdot (h\bar{\boldsymbol{u}}) = w_e - w_d, \tag{3}$$

$$\frac{\partial}{\partial t}(h\bar{\boldsymbol{u}}) + \nabla \cdot (h\bar{\boldsymbol{u}} \otimes \bar{\boldsymbol{u}}) + \nabla \left(\frac{1}{2} g_z h^2\right) = h\boldsymbol{S}, \tag{4}$$

where $\cdot$, $\otimes$ and $\nabla = (\partial/\partial x, \partial/\partial y)$ are the two-dimensional scalar product, the dyadic product and the gradient operator, respectively. The erosion and deposition rates are w_e and w_d, respectively. The source term $\boldsymbol{S}$ includes contributions from gravity and effective friction,

$$\boldsymbol{S} = \boldsymbol{g}_{||} - \mu(I) g_z \boldsymbol{e}, \tag{5}$$

where μ is the friction coefficient, $\boldsymbol{g}_{||} = (g_x, g_y)$ are the x, y components of the gravitational acceleration vector and $\boldsymbol{i}$, $\boldsymbol{j}$ are the orthogonal unit vectors aligned with the input topography projection lines. The frictional force is oriented opposing the direction of flow, which is defined as

$$\boldsymbol{e} = \begin{cases} \dfrac{\bar{\boldsymbol{u}}}{|\bar{\boldsymbol{u}}|}, & |\bar{\boldsymbol{u}}| > 0, \\ \dfrac{|\boldsymbol{g}_{||}|/g_z\, \boldsymbol{i} - \nabla h}{||\boldsymbol{g}_{||}|/g_z\, \boldsymbol{i} - \nabla h|}, & |\bar{\boldsymbol{u}}| = 0. \end{cases} \tag{6}$$

Where the material is stationary, the frictional force acts to oppose the resulting force due to gravity and the depth-averaged pressure gradient. Where $|\bar{\boldsymbol{u}}| = (\bar{u}^2 + \bar{v}^2)^{1/2}$ is non-zero, the frictional force opposes the direction of motion.

2.2 The hysteretic basal friction law

A Froude number is defined to be the ratio of the bulk velocity to the gravitational wave speed and links the steady uniform flow speed of the avalanche to the thickness through a flow rule for angular granular materials (Pouliquen and Forterre, 2002; Forterre and Pouliquen, 2003; Edwards et al., 2017, 2019),

$$Fr = \frac{|\bar{\boldsymbol{u}}|}{\sqrt{g_z h}} = \beta \frac{h}{h_{\text{stop}}} - \Gamma. \tag{7}$$

The material parameters β, β_* and Γ are determined by fits to this empirical flow law. The friction angles $\mu_1 = \tan\zeta_1$, $\mu_2 = \tan\zeta_2$, $\mu_3 = \tan\zeta_3$, and the frictional length scale $\mathscr{L}$ are found by experimental fits to the curves,

$$h_{\text{stop}}(\zeta) = \mathscr{L}\left(\frac{\tan\zeta_2 - \tan\zeta_1}{\tan\zeta - \tan\zeta_1} - 1\right), \tag{8}$$

$$h_{\text{start}}(\zeta) = \mathscr{L}\left(\frac{\tan\zeta_2 - \tan\zeta_1}{\tan\zeta - \tan\zeta_3} - 1\right), \tag{9}$$

which define the deposit depth of a steady uniform flow at a slope angle ζ and the corresponding activation thickness for a given slope angle, respectively.

The non-monotonic friction law then describes the hysteretic behaviour of grains and consists of dynamic, intermediate and static regimes (Edwards et al., 2019),

$$\mu(h, Fr) = \begin{cases} \mu_D, & Fr \geq \beta_*, \\ \mu_I, & 0 < Fr < \beta_*, \\ \mu_S, & Fr = 0, \end{cases} \tag{10}$$

which are defined by the functions

$$\mu_D = \mu_1 + \frac{\mu_2 - \mu_1}{1 + h\beta/(\mathscr{L}(Fr + \Gamma))}, \tag{11}$$

$$\mu_I = \left(\frac{Fr}{\beta_*}\right)\left(\mu_1 + \frac{\mu_2 - \mu_1}{1 + h\beta/(\mathscr{L}(\beta_* + \Gamma))} - \mu_3 - \frac{\mu_2 - \mu_1}{1 + h/\mathscr{L}}\right) + \mu_3 + \frac{\mu_2 - \mu_1}{1 + h/\mathscr{L}}, \tag{12}$$

$$\mu_S = \min\left(|\tan\zeta\, \boldsymbol{i} - \nabla h|,\ \mu_3 + \frac{\mu_2 - \mu_1}{1 + h/\mathscr{L}}\right). \tag{13}$$

The minimum dynamic friction is assumed to occur at a constant Froude number $Fr = \beta_*$, which has a corresponding transition thickness $h_* = (\beta_* + \Gamma)h_{\text{stop}}/\beta$ and is a multiple of $h_{\text{stop}}(\zeta)$. Following Russell et al. (2019) and Edwards et al. (2019), the frictional transition in the intermediate regime is assumed to be linear.

Figure 2 shows the friction law described in (10) parameterised with values for dense snow as in table 1:2. The friction is multivalued at $Fr = 0$ up to

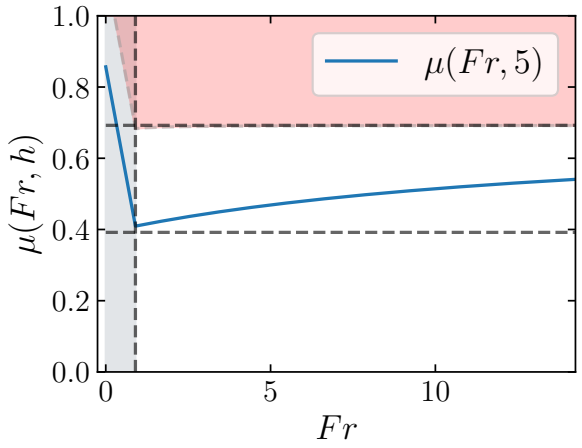


Fig. 2: Shows the $\mu(Fr, h)$ friction law parameterised with values from dense snow (see table 1:2). The red region depicts flows with thickness less than a grain diameter and is, therefore, unreachable. The grey region depicts the transition zone between static (multivalued) frictional behaviour and dynamic frictional behaviour. The blue line shows values of the effective friction for a dense avalanche of thickness 5 m.

a value for μ_{start} where all material is assumed to start flowing. For values of $Fr > \beta_*$, the friction is bounded between two threshold values; a minimum value such that any flow with thickness less than h_* has to decelerate or stop, and an upper maximal value, above which all flows are accelerating and cannot reach a steady uniform state (Pouliquen, 1999).

2.3 *The parameterisation for dry snow*

Following deposition measurements at the Vallée de la Sionne test site in Switzerland, it has been shown that the partial parameterisation of the friction law (10) is possible for snow avalanches, see Sovilla et al. (2010). In the study, the authors show that $h_{\text{stop}}(\zeta)$ measurements can be parameterised by the empirical description given in (8), which allows us to take values for ζ_1, ζ_2 and $\mathscr{L}$ from these measurements for an idealised snow parameterisation.

Values for the other frictional parameters have yet to be verified by experiments. However, measurements of deposit depths from instantaneous velocities at specific locations would allow an approximation for the β and Γ parameters to be found under the substantial assumption that the avalanche does not deviate greatly from its steady uniform flow solution at a given slope angle. A further challenge

Table 1: Material friction parameters for snow used in this study with $\zeta_{1,2}$ and $\mathscr{L}$ inferred from Sovilla et al. (2010).

ID	*Set Name*	*Frictional Parameters*
1	Voellmy Params.	$\mu = 0.4$, $k = g/\xi = 0.004$
2	Idealised Snow 1	$\zeta_1 = 21.4°$, $\zeta_2 = 34.7°$, $\zeta_3 = 40.0°$, $\beta = 0.9$, $\beta_* = 0.9$, $\mathscr{L} = 0.31$ m, $\kappa = 1$, $\Gamma = 0.0$
3	Idealised Snow 2	$\zeta_1 = 21.4°$, $\zeta_2 = 34.7°$, $\zeta_3 = 40.0°$, $\beta = 9.0$, $\beta_* = 0.9$, $\mathscr{L} = 0.31$ m, $\kappa = 1$, $\Gamma = 0.0$

is that for lower slope angles $h_{\text{stop}}(\zeta)$ is infinite, see figure 3, *i.e.* large layers of material on a plane of that slope angle will not flow. This limits the range of slope angles on which measurements can be taken from in order to parameterise the curve.

Given the lack of experimental data for these material parameters (that the authors are aware of), in this paper we have used measurements from the Ryggfonn test site to approximate values for β, β_* and Γ, such that similar runout values and velocities are given across all test simulations.

For dry granular materials, the ζ_3 parameter can be found by measuring the slope angle ζ_{start} at which failure of metastable layers of thickness h occurs. The relation (9) is then given by the inverse of the $\zeta_{\text{start}}(h)$ curve. For snow, however, cohesion of static material additionally plays a role in the metastable state of the layer, and thus, the same approach would not capture the behaviour. Mathematically, however, using this relation allows metastable layers to exist and the interaction and transition from the static to moving material to be captured by the model. In view of this, a value of $\mu_3 = \tan(40°)$ was chosen to approximate the behaviour of avalanches typically failing between a 30°–50° slope angle.

2.4 *The numerical implementation*

The system of equations (3)–(4) is solved for the thickness and the velocity fields using a finite volume method for hyperbolic conservation equations, namely a strongly simplified variant of the method of transport (*MoT*) (Fey, 1998). Applications using this scheme have shown good results for avalanche simulations utilising the Voellmy friction law. The efficiency has allowed the method to be utilised in regional scale and probabilistic-based studies (Issler et al., preprint). The scheme has been adapted in

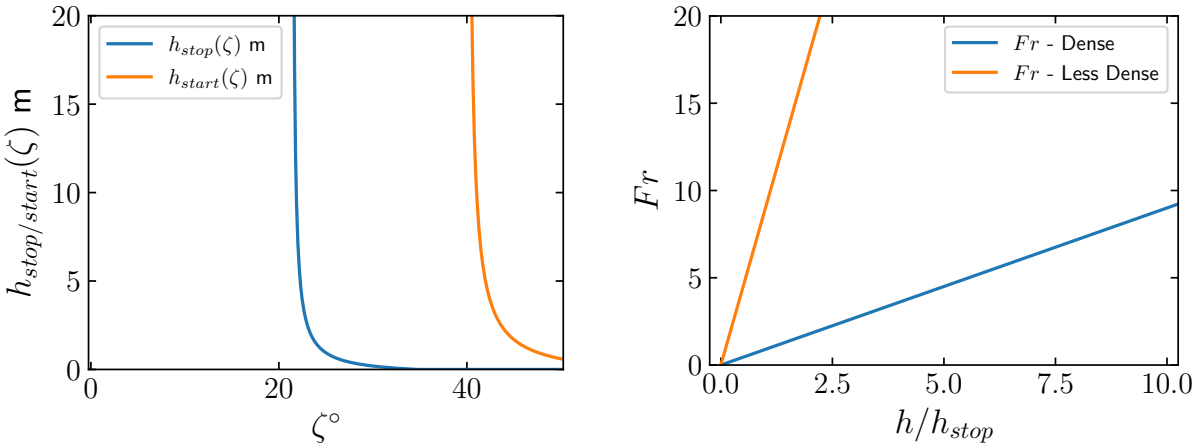


Fig. 3: Left: Shows $h_{\text{stop}}(\zeta)$ and $h_{\text{start}}(\zeta)$ curves for the simulated snow parameters (table 1:2). Right: Shows the flow rule for Fr in terms of h and $h_{\text{stop}}(\zeta)$, assuming granular behaviour of a dense snow avalanche for two distinct snow avalanche parameterisations tested (table 1:2,3).

this study to include the hysteretic friction law and to manage the stopped material behaviour. Typically for geophysical applications, DEM data takes a cell size of 5–10 m, with the simulations in section 3.1 taking a 5 m grid.

In order to achieve stable integration of the hyperbolic system of equations, a maximum time step, given by a CFL (Courant–Friedrichs–Lewy) condition, is used with a CFL number of 0.8 (LeVeque, 2002). The release area is applied via a mask to the topography DEM and given a specified fracture depth of 3 m.

For simplicity, in the following simulations, the difference in erosion and deposition rates $w_e - w_d$ (r.h.s. of (3)) is assumed to be zero. The code implements von Neumann (outflow) conditions on the domain boundaries, however, in all the simulations presented, flowing material is not expected to interact with the boundary.

3 RESULTS

3.1 *Model comparison to Ryggfonn experiments*

Simulations were run for three prototypical historic avalanches at the Ryggfonn test site in Norway (Lied et al., 2004). Three distinct runout types were chosen; (i) a short runout that stops in the upper section of the path (30.04.2016), (ii) an avalanche that reaches and is diverted by the dam (11.04.1988) and (iii) an avalanche that overtops the dam by a substantial distance (28.01.1987). Release areas were applied to the simulations from observations of the avalanches and given a fracture-depth value of 3 m. All three tests use the same parameterisation for an idealised dense snow as given in table 1:2 and described in section 2.3. In each of the figures 4–7, the avalanches maximum thickness at each cell is shown alongside the maximum speed at each cell over the duration of the experiment. This gives a good indication of the extent of the avalanche and of the avalanche mobility.

Figure 4 shows a short avalanche from a small release area that was triggered by explosives. The model is able to capture the short runout of the material that arests in the upper bowl. The stopped material considerations in the model come into play here, with shallower material (due to the smaller release area volume) leading to the deposition regime in the friction law. This allows material to be held on the low slope angle area in the upper bowl where larger flows would be able to pass over. The simulation captures the short runout with reasonable deposit depths, given the size of the avalanche, and the highest speeds calculated are around 30 ms^{-1}.

Figure 5 shows a moderately large avalanche that reached the dam from a substantial release area that was again triggered by explosives. Here the differing flow behaviour is captured and the flow is intercepted by the dam. The main deposition features of the build up behind the dam are captured by the model, however, for this paramterisation the avalanche is not diverted around the right hand edge of the dam. In this case the model predicts a fairly sustained speed of around 35 ms^{-1}.

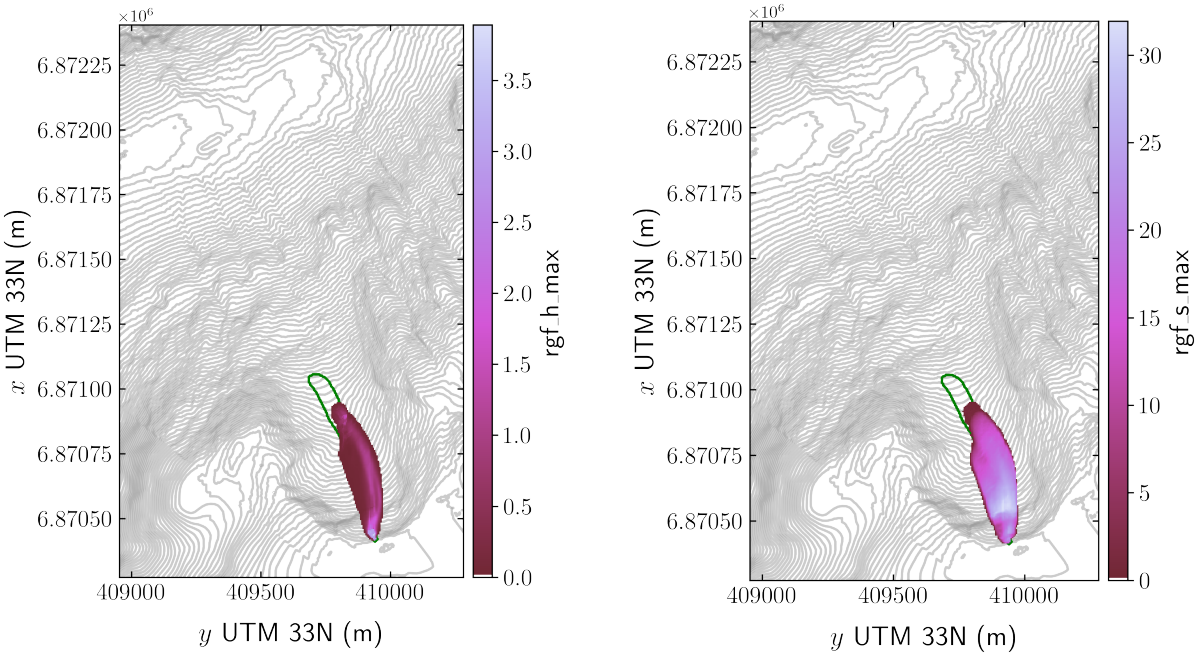


Fig. 4: Simulation results of the max-per-cell thickness (m) and max-per-cell speed (ms^{-1}) over the simulation duration for the 30.04.2016 avalanche. The green outline shows the observed extent of the avalanche. Here the short runout is captured using the table 1:2 material parameterisation but not its full extent. Reasonable values for the deposit thickness and avalanche speed are shown.

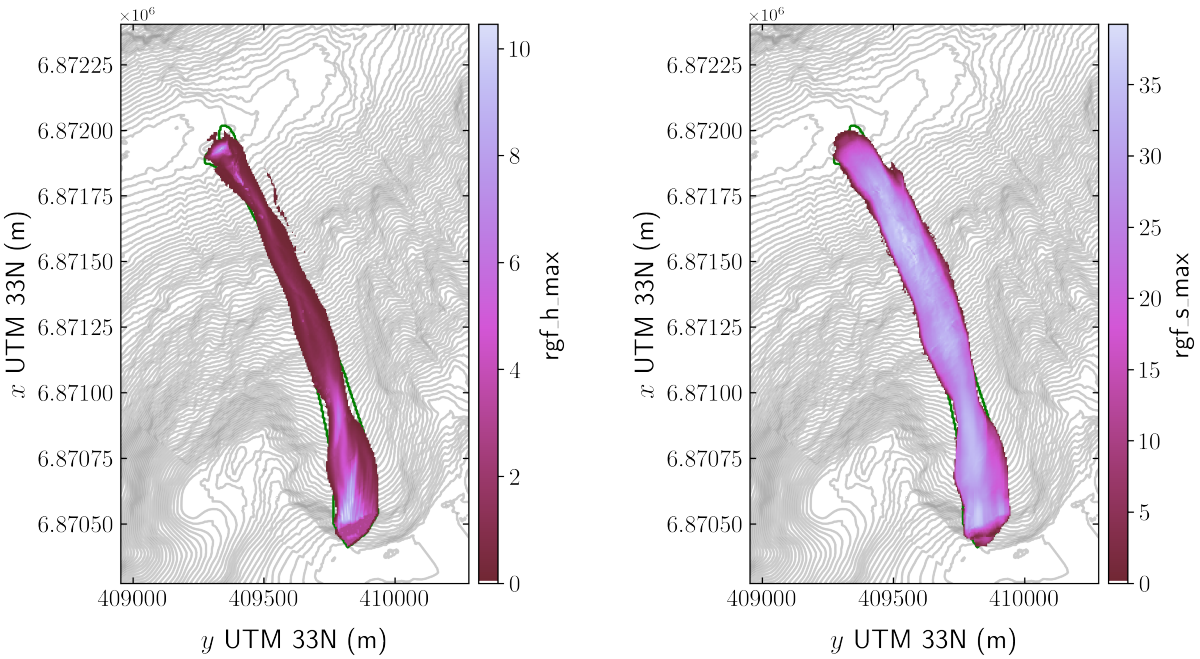


Fig. 5: Plot symbols as for figure 4 for the 11.04.1988 avalanche. Here the behaviour of the runout hitting and stopping at the dam is captured using the table 1:2 material parameterisation.

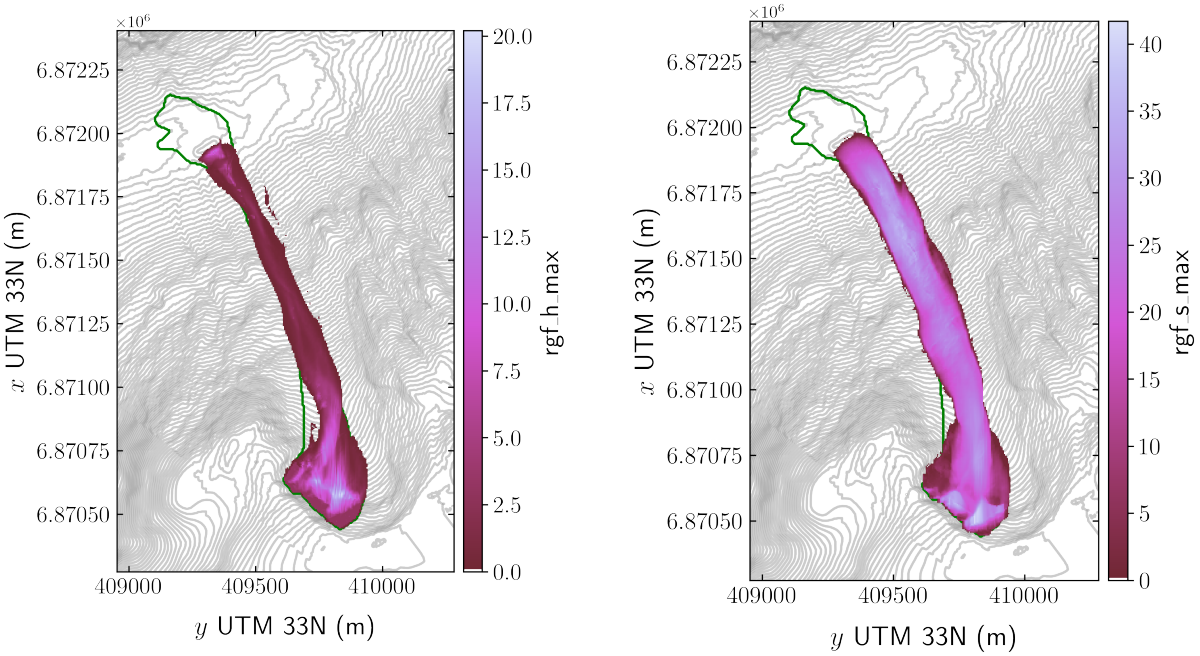


Fig. 6: Plot symbols as for figure 4 for the 28.01.1987 avalanche. Here the behaviour of the avalanche overtopping the dam is not captured. This is likely, due to the dense flow paramterisation.

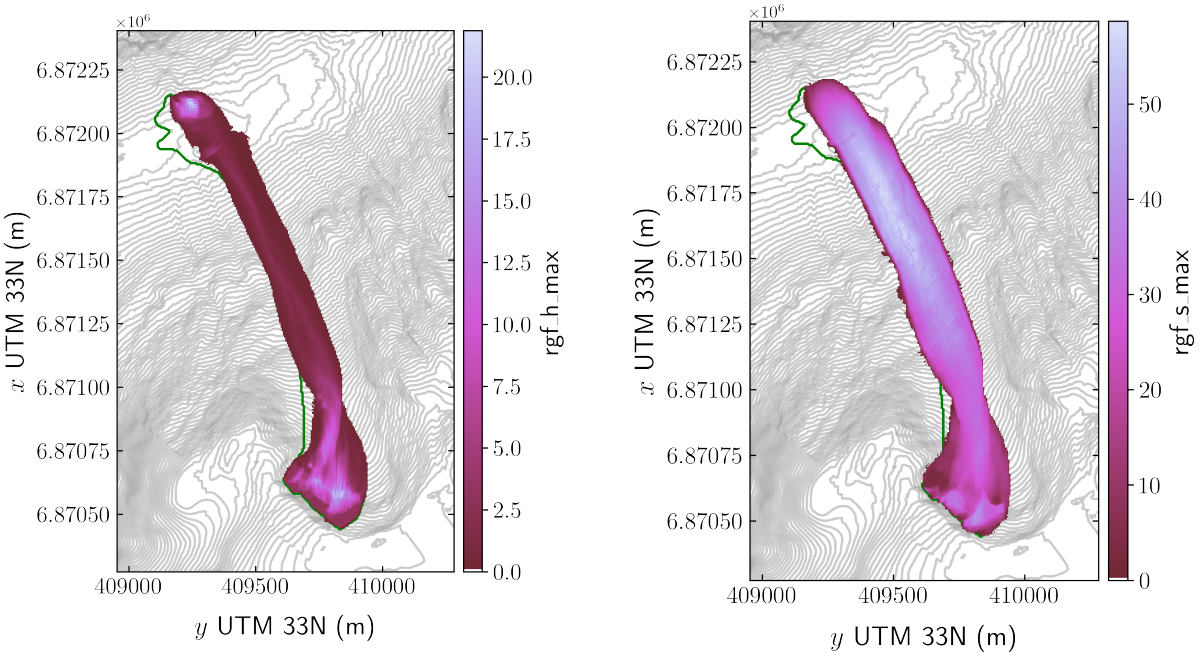


Fig. 7: Plot symbols as for figure 4 with initial conditions and extent identical to figure 6. In this case the parameters are adjusted to force the flow to overtop the dam (table 1:3). This indicates paramterisation for less dense avalanches are able to be captured with the model.

Finally in figure 6 a large fluidised avalanche is shown that was naturally released and overtopped the dam leaving a large area of deposit both in front of and behind the dam. In this case the simulation is not able to capture this behaviour and the material is stopped by the dam. A sustained speed of around $40\,\mathrm{ms}^{-1}$ is captured for the dense flow. Figure 7 shows how the model parameters can be adjusted to a more fluidised avalanche regime where material overtops the dam (table 1:3). While undoubtedly more work is required to include a fluidisation processes in such a model, these initial experiments show promise to capture such effects in a physical way.

4 DISCUSSION AND CONCLUSIONS

By utilising a friction law with an idealised parameterisation for snow, we are able to capture three distinct behaviours of historic avalanches at the Ryggfonn test site. This shows that the rheological model has significant potential as key features of the avalaches are captured using an idealised parameterisation.

The model aditionally has scope to be extended beyond dense flows and into more complex regimes where interstitial fluid plays a role in the flow dynamics. The model has seen depth-averaged extensions that allow it to cope well with the quasi-static shearing regime as the avalanche transitions between a stationary and a flowing state (Russell et al., 2019; Rocha et al., 2019; Tregaskis et al., 2022). Advances have recently been proposed towards using an extended version of the rheology in pyroclastic density currents, where the rapid collisional regime at high speeds is important for the flow dynamics (Holyoake and McElwaine, 2012; Barker et al., 2021; Breard et al., 2022). This is a similar regime to fluidisation process observed in rapid dry snow avalanches.

In this paper we show that a material-based parmterisation in a depth averaged model is capable of capturing many key avalanche properties and shows significant promise towards future extentions including more complex avalanche phenomena.

ACKNOWLEDGEMENTS

This work was carried out within the project Applied Avalanche Research in Norway (AARN), which is financed by the Norwegian Department of Petroleum and Energy (OED) through a special grant for avalanche research at NGI, administrated by the Norwegian Water Resources and Energy Directorate (NVE). The authors would like to thank Nico Gray and Chris Johnson at the University of Manchester for their contributions towards this research.

REFERENCES

Barker, T., Rauter, M., Maguire, E. S. F., Johnson, C. G., and Gray, J. M. N. T.: Coupling rheology and segregation in granular flows, J. Fluid Mech., 909, 2021.

Breard, E. C. P., Fullard, L., Dufek, J., Tennenbaum, M., Fernandez-Nieves, A., and Dietiker, J.-F.: Investigating the rheology of fluidized and non-fluidized gas-particle beds: implications for the dynamics of geophysical flows and substrate entrainment, Granul. Matter, 24, 1–25, 2022.

Eckert, N., Parent, E., Kies, R., and Baya, H.: A spatio-temporal modelling framework for assessing the fluctuations of avalanche occurrence resulting from climate change: application to 60 years of data in the northern French Alps, Clim. Change, 101, 515–553, 2010.

Edwards, A. N. and Gray, J. M. N. T.: Erosion-deposition waves in shallow granular free-surface flows, J. Fluid Mech., 762, 35–67, 2015.

Edwards, A. N., Viroulet, S., Kokelaar, B. P., and Gray, J. M. N. T.: Formation of levees, troughs and elevated channels by avalanches on erodible slopes, J. Fluid Mech., 823, 278–315, 2017.

Edwards, A. N., Russell, A., Johnson, C. G., and Gray, J. M. N. T.: A non-monotonic friction law for hysteresis in dry granular avalanches, J. Fluid Mech., 875, 1058–1095, 2019.

Fey, M.: Multidimensional upwinding. Part I. The method of transport for solving the Euler equations, J. Comput. Phys., 143, 159–180, 1998.

Forterre, Y. and Pouliquen, O.: Long-surface-wave instability in dense granular flows, J. Fluid Mech., 486, 21–50, 2003.

GDR-MiDi: On dense granular flows, Eur. Phys. J. E, 14, 341–365, 2004.

Gray, J. M. N. T. and Edwards, A. N.: A depth-averaged $\mu(I)$-rheology for shallow granular free-surface flows, J. Fluid Mech., 755, 503–544, 2014.

Holyoake, A. J. and McElwaine, J. N.: High-speed granular chute flows, J. Fluid Mech., 710, 35–71, 2012.

Issler, D., Gisnås, K. G., Gauer, P., Glimsdal, S., Domaas, U., and Sverdrup-Thygeson, K.: Naksin–a New Approach to Snow Avalanche Hazard Indication Mapping in Norway, preprint on webpage at `https://papers.ssrn.com/sol3/papers.cfm?abstract_id=4530311`, preprint.

LeVeque, R. J.: Finite Volume Methods for Hyperbolic Problems, Cambridge University Press, 2002.

Lied, K., Moe, A., Kristensen, K., and Issler, D.: Ryggfonn. Full scale avalanche test site and the effect of the catching dam, in: Snow and avalanches test sites, edited by Naaim, M. and Naaim-Bouvet, F., Cemagref Editions, 2004.

Pouliquen, O.: Scaling laws in granular flows down rough inclined planes, Phys. Fluids, 11, 542–548, 1999.

Pouliquen, O. and Forterre, Y.: Friction law for dense granular flows: application to the motion of a mass down a rough inclined plane, J. Fluid Mech., 453, 133–151, 2002.

Rocha, F. M., Johnson, C. G., and Gray, J. M. N. T.: Self-channelisation and levee formation in monodisperse granular flows, J. Fluid Mech., 876, 591–641, 2019.

Russell, A., Johnson, C. G., Edwards, A. N., Viroulet, S., Rocha, F. M., and Gray, J. M. N. T.: Retrogressive failure of a static granular layer on an inclined plane, J. Fluid Mech., 869, 313–340, 2019.

Sovilla, B., McElwaine, J. N., Schaer, M., and Vallet, J.: Variation of deposition depth with slope angle in snow avalanches: Measurements from Vallée de la Sionne, J. Geophys. Res.: Earth Surface, 115, F02 016, 2010.

Tregaskis, C., Johnson, C. G., Cui, X., and Gray, J. M. N. T.: Subcritical and supercritical granular flow around an obstacle on a rough inclined plane, J. Fluid Mech., 933, 2022.

Voellmy, A.: Über die Zerstörungskraft von Lawinen, Schweiz. Bauzeitung, 73, 159–165, 212–217, 246–249, 280–285, 1955.